

Joint Detection and Angle Estimation for Multiple Jammers in Beam-space Massive MIMO

Pengguang Du^{1,2}, Cheng Zhang^{1,2}, Changwei Zhang², Zhilei Zhang², Yongming Huang^{1,2}

¹National Mobile Communications Research Laboratory, School of Information of Science and Engineering, Southeast University, Nanjing 210096, China.

²Purple Mountain Laboratories, Nanjing 211111, China.

Email: {pgdu, zhangcheng_seu, huangym}@seu.edu.cn, {zhangchangwei, zhangzhilei}@pmlabs.com.cn

Abstract—In this paper, we study the joint detection and angle estimation problem for beam-space multiple-input multiple-output (MIMO) systems with multiple random jamming targets. An iterative low-complexity generalized likelihood ratio test (GLRT) is proposed by transforming the composite multiple hypothesis test on the projected vector into a series of binary hypothesis tests based on the spatial covariance matrix. In each iteration, the detector implicitly inhibits the mainlobe effects of the previously detected jammers by utilizing the estimated angles and average jamming-to-signal ratios. This enables the detection of a new potential jammer and the identification of its corresponding spatial covariance. Simulation results demonstrate that the proposed method outperforms existing benchmarks by suppressing sidelobes of the detected jammers and interference from irrelevant angles, especially in medium-to-high jamming-to-noise ratio scenarios.

Index Terms—Beam-space massive MIMO, joint detection and estimation, generalized likelihood ratio test, spatial covariance identification.

I. INTRODUCTION

Beam-space multiple-input multiple-output (MIMO) utilizes directional beams and jamming nulling techniques to effectively isolate jamming signals, significantly enhancing the system's resilience to jamming and improving spectral efficiency, making it particularly well-suited for jamming-intensive environments and spectrum-constrained scenarios [1]. However, the design of spatial beams relies on prior information about the jammers, such as the presence of the jammer and the instantaneous or statistical characteristics of the jamming channel [1]–[3]. To effectively mitigate jamming effects, jamming detection and parameter estimation have become imperative [2]–[6].

The problem of jamming detection in traditional spatial-domain MIMO systems has been studied, with several techniques proposed, including eigen-decomposition [4], the generalized likelihood ratio test (GLRT) [5], and phase detection of the inner-product [6]. However, these approaches primarily focus on detecting the presence of jammers but fail to estimate the number of unknown jammers. In addition, these methods often suffer from performance degradation when applied to millimeter-wave (mmWave) channels with spatial correlation. As mentioned in [7], the detection probability of the GLRT in a rank-1 channel with strong correlation drops to less than half of that in a full-rank channel at low false-alarm probability. In terms of jamming parameter estimation, the authors of [8] and [9] aim to estimate the jamming channel using the

minimum mean square error (MMSE) criterion. Other studies take advantage of the angular domain knowledge by using the angular subspace of the jammer to estimate the path gain and channel state information (CSI) [10]. These CSI estimation methods rely heavily on statistical information, such as the spatial covariance matrix [9] or the channel subspace [10]. However, in beam-space MIMO, the limited number of radio frequency (RF) chains results in insufficient spatial resolution, preventing the base station (BS) from accurately identifying the jamming subspace using conventional techniques.

Given the challenges outlined above, the development of an algorithm for joint jamming detection and parameter estimation is essential. This problem has recently been studied in the context of distributed MIMO radars using the generalized information criterion (GIC) [11], [12]. The main difference between this study and existing works is that the jamming is assumed to be an unknown random signal, while the radar waveform is predetermined. This distinction prevents the scheme in [11] from obtaining a tractable closed-form expression for the optimization objective through the maximum likelihood estimation (MLE) of the CSI, making it a non-optimal solution. Building on these related studies, we make the following contributions:

- The joint jamming detection and angle estimation (JDAE) problem is formulated using the projected vector obtained by pilot space projection, which contain only the jamming signals and not the user signals. We derive the likelihood function of the projected vector and establish its relationship with the spatial angles. It is then shown that the GIC-based detector is infeasible for this scenario.
- By transforming the multiple hypothesis test into multiple binary hypothesis tests, an iterative low-complexity GLRT scheme based on spatial covariance identification (SCI) is proposed. In each iteration, the detector suppresses the mainlobes of previously detected jammers and identifies a new potential jammer and estimate its covariance matrix.
- Finally, we evaluate the performance of the proposed detector against benchmarks to validate its effectiveness. Simulation results show that the proposed method has significant differences in the detection metrics between jamming targets and irrelevant angles, and exhibits excel-

lent performance in the medium-to-high interference-to-noise ratio (JNR) region. Specifically, at a JNR of 15 dB, the detection probability increases by 23.16% compared to the benchmark with the best performance.

II. SYSTEM MODEL AND PILOT-SPACE PROJECTION

Consider an uplink beamspace massive MIMO communication system, where a BS is equipped with M antennas and N RF chains, serving K single-antenna users simultaneously via orthogonal frequency division multiple access. In this system, J jammers within the coverage area attempt to disrupt the uplink training by transmitting jamming signals. Each jammer is equipped with M' antennas and a single RF chain [13].

During the uplink training phase, the users transmit pilot sequences to the BS. Denote the set of pilots in the system as $\Phi = \{\phi_1, \dots, \phi_\tau\}$ where $\phi_i \in \mathbb{C}^{\tau \times 1}$, and τ is the pilot length. The pilot sequences are mutually orthogonal, and the powers of the pilots are normalized such that $\|\phi_i\|^2 = \tau, \forall i \in \{1, \dots, \tau\}$. Since each user occupies a different subcarrier, the BS can perfectly distinguish the signals from individual users. For simplicity, we consider the case of a single subcarrier (i.e., one user). We assume that the user transmits the pilot sequence with index 1, while the BS uses an analog RF combiner $\mathbf{W} \in \mathbb{C}^{M \times N}$ to observe the received signal. Meanwhile, the j -th jammer transmits a jamming pilot sequence ψ_j with an analog beamforming vector $\mathbf{u}_j \in \mathbb{C}^{M' \times 1}$, where $\psi_j \sim \mathcal{CN}(\mathbf{0}, \mathbf{I}_\tau)$ and is independent for different j . The received signal matrix at the BS can be written as follows:

$$\mathbf{Y} = \sqrt{P}\mathbf{W}^H\mathbf{h}\phi_1^T + \sum_{j=1}^J \sqrt{Q_j}\mathbf{W}^H\mathbf{H}_j\mathbf{u}_j\psi_j^T + \mathbf{W}^H\mathbf{N}, \quad (1)$$

where P and Q_j are the pilot powers of the user and jammer j , respectively. $\mathbf{N} \in \mathbb{C}^{N \times \tau}$ denotes the additive noise matrix, where the elements are assumed to be zero-mean complex Gaussian random variables with unit-variance. $\mathbf{h} \in \mathbb{C}^{M \times 1}$ is the channel vector between the BS and the user, and $\mathbf{H}_j \in \mathbb{C}^{M \times M'}$ is the channel matrix from jammer j to the BS.

We assume an unobstructed direct path between the user or jammer and the BS, which is relevant to scenarios such as mmWave communications for unmanned aerial vehicles (UAVs) [14] and vehicle-to-everything (V2X) networks [15]. In this case, \mathbf{h} and \mathbf{H}_j can be written as

$$\mathbf{h} = \beta\mathbf{a}(\theta), \text{ and } \mathbf{H}_j = \beta_j\mathbf{a}(\theta_j)\mathbf{a}_j^H(\phi_j), \quad (2)$$

where β and β_j denote the fading coefficients of the user and jammer j to the BS, θ and θ_j represent the angles of arrival for the user and jammer j , and ϕ_j is the departure angle of jammer j . The vector $\mathbf{a}(\theta)$ is the array response vector for the BS. For a typical uniform linear array (ULA) with half-wavelength antenna spacing, the m -th element of $\mathbf{a}(\theta)$ can be written as $[\mathbf{a}(\theta)]_m = \frac{1}{\sqrt{M}}e^{-j\pi m\theta}$, where $\theta = \sin(\varphi)$ and φ is the physical angle. The array response vector for the jammer $\mathbf{a}_j(\phi)$ can be derived in a similar way.

The signal preprocessing scheme based on the pilot-space projection is briefly described next. Under a priori knowledge

of the pilot set Φ , the BS post-multiplies the received signal \mathbf{Y} by ϕ_i^* and normalizes it by \sqrt{P} and τ to obtain

$$\mathbf{y}_i = \mathbf{W}^H\mathbf{h}\delta(i-1) + \sum_{j=1}^J \sqrt{\frac{Q_j}{P}}\alpha_{j,i}\mathbf{W}^H\mathbf{H}_j\mathbf{u}_j + \mathbf{n}_i, \quad (3)$$

where $\delta(i)$ is the Dirac delta function, and $\alpha_{j,i} = \frac{1}{\tau}\psi_j^T\phi_i^*$ is the inner-product of the random jamming pilot vector from jammer j and the i -th legitimate pilot vector. The vector $\mathbf{n}_i = \frac{1}{\sqrt{P}\tau}\mathbf{W}^H\mathbf{N}\phi_i^*$ denotes the equivalent noise projected onto the i -th pilot, with the elements being independent and identically distributed following $\mathcal{CN}(0, \sigma^2)$, where the variance $\sigma^2 = \frac{1}{P\tau}$, and \mathbf{n}_i is independent for different i [7].

According to (2), the beamforming gain of the jammer is absorbed into the fading coefficient, yielding $\tilde{\beta}_j = \beta_j\mathbf{a}_j^H(\phi_j)\mathbf{u}_j$. Denote the index set of the unused pilots as $\mathbf{t} = \{2, \dots, \tau\}$ with cardinality τ' . Based on (3), the projected vector corresponding to an unused pilot with index i is given by

$$\mathbf{y}_i = \mathbf{W}^H \sum_{j=1}^J \sqrt{\frac{Q_j}{P}}\alpha_{j,i}\tilde{\beta}_j\mathbf{a}(\theta_j) + \mathbf{n}_i, i \in \mathbf{t}. \quad (4)$$

By defining the array response matrix $\mathbf{A} = [\mathbf{a}(\theta_1), \dots, \mathbf{a}(\theta_J)]$, we can express \mathbf{y}_i in an alternative form: $\mathbf{y}_i = \mathbf{W}^H\mathbf{A}\alpha_i + \mathbf{n}_i$ for $i \in \mathbf{t}$, where $\alpha_i = [\tilde{\alpha}_{i,1}, \dots, \tilde{\alpha}_{i,J}]^T \in \mathbb{C}^{J \times 1}$ represents the equivalent jamming gain vector, and $\tilde{\alpha}_{i,j} = \sqrt{\frac{Q_j}{P}}\alpha_{i,j}\tilde{\beta}_j$.

We then combine the projected vectors corresponding to all unused pilots into a new vector $\mathbf{y} = [\mathbf{y}_2^T, \dots, \mathbf{y}_\tau^T]^T \in \mathbb{C}^{\tau' \times N \times 1}$. Specifically, it can be represented as

$$\mathbf{y} = \text{blk} \left\{ \mathbf{W}^H\mathbf{A}, \dots, \mathbf{W}^H\mathbf{A} \right\} \boldsymbol{\beta} + \mathbf{n} = \left(\mathbf{I}_{\tau'} \otimes \mathbf{W}^H\mathbf{A} \right) \boldsymbol{\beta} + \mathbf{n}, \quad (5)$$

where $\boldsymbol{\beta} = [\alpha_2^T, \dots, \alpha_\tau^T]^T \in \mathbb{C}^{\tau' \times J \times 1}$, $\mathbf{n} = [\mathbf{n}_2^T, \dots, \mathbf{n}_\tau^T]^T$, and the symbol \otimes denotes the Kronecker product.

III. JOINT DETECTION AND ANGLE ESTIMATION FOR MULTIPLE JAMMERS

In this section, we first formulate the JDAE problem for multiple jammers in beamspace MIMO using the projected vector. On this basis, we demonstrate the infeasibility of the GIC-based scheme by deriving the likelihood function of the projected vector. Finally, an iterative GLRT scheme based on spatial covariance identification is proposed.

A. Formulation of the Hypothesis Testing Problem

Given the projected vector \mathbf{y} , our goal is to simultaneously determine the number of unknown jammers and estimate their respective angles. Based on (5), this leads to a composite multiple hypothesis testing problem, which is defined as follows:

$$\begin{cases} \mathcal{H}_0 : & \mathbf{y} = \mathbf{n}, \\ \mathcal{H}_1 : & \mathbf{y} = \left(\mathbf{I}_{\tau'} \otimes \mathbf{W}^H\mathbf{a}(\theta_1) \right) \boldsymbol{\beta}_{1:1} + \mathbf{n}, \\ & \vdots \\ \mathcal{H}_{J_{\max}} : & \mathbf{y} = \left(\mathbf{I}_{\tau'} \otimes \mathbf{W}^H\mathbf{A}(\theta_{1:J_{\max}}) \right) \boldsymbol{\beta}_{1:J_{\max}} + \mathbf{n}, \end{cases} \quad (6)$$

where \mathcal{H}_0 represents the null hypothesis, and \mathcal{H}_j corresponds to the hypothesis of j jammers being present. Under $\mathcal{H}_j, j = 1, \dots, J_{\max}$, the unknown spatial angle vector of j jammers is denoted as $\boldsymbol{\theta}_{1:j} = [\theta_1, \dots, \theta_j]^\top$, and the corresponding array response matrix is $\mathbf{A}(\boldsymbol{\theta}_{1:j}) = [\mathbf{a}(\theta_1), \dots, \mathbf{a}(\theta_j)]$. The unknown jamming gain vector is represented as $\boldsymbol{\beta}_{1:j} = [\alpha_{2,1:j}^\top, \dots, \alpha_{\tau,1:j}^\top]^\top$, where $\alpha_{i,1:j}$ contains the first j elements of α_i . The maximum possible number of jammers is constrained by $J_{\max} \geq 1$.

The likelihood function of the projected vector \mathbf{y} is analyzed next. Based on the assumption regarding the jamming pilot sequence $\boldsymbol{\psi}_j$ in (1), the gain vector α_i or $\boldsymbol{\beta}$ is known to follow a complex Gaussian distribution. During the training interval, the channels are treated as deterministic, so \mathbf{y} is a complex Gaussian vector. Under $\mathcal{H}_j, j = 1, \dots, J_{\max}$, the log-likelihood function is expressed as follows:

$$\ln f_j(\mathbf{y}; \boldsymbol{\theta}_{1:j}, \Upsilon_{1:j}) = -\tau' N \ln \pi - \ln |\mathbf{R}_y| - \mathbf{y}^H \mathbf{R}_y^{-1} \mathbf{y}, \quad (7)$$

where $\Upsilon_{1:j} = \mathbb{E}[\boldsymbol{\beta}_{1:j} \boldsymbol{\beta}_{1:j}^H]$ is the self-covariance matrix of $\boldsymbol{\beta}_{1:j}$, and \mathbf{R}_y is the self-covariance matrix of \mathbf{y} , given by:

$$\mathbf{R}_y = [\mathbf{I}_{\tau'} \otimes \boldsymbol{\Psi}(\boldsymbol{\theta}_{1:j})] \Upsilon_{1:j} [\mathbf{I}_{\tau'} \otimes \boldsymbol{\Psi}(\boldsymbol{\theta}_{1:j})]^H + \sigma^2 \mathbf{I}_{\tau' N}, \quad (8)$$

where $\boldsymbol{\Psi}(\boldsymbol{\theta}_{1:j}) = \mathbf{W}^H \mathbf{A}(\boldsymbol{\theta}_{1:j}) \in \mathbb{C}^{N \times j}$. For $\mathbf{m} = [(m-2)j + 1, \dots, (m-1)j]$ and $\mathbf{n} = [(n-2)j + 1, \dots, (n-1)j]$, $\forall m, n \in \mathfrak{t}$, $[\Upsilon_{1:j}]_{\mathbf{m}, \mathbf{n}} = \mathbb{E}[\alpha_{m,1:j} \alpha_{n,1:j}^H]$ is the $(m-1, n-1)$ -th block of the matrix $\Upsilon_{1:j}$. The (t, s) -th element of $[\Upsilon_{1:j}]_{\mathbf{m}, \mathbf{n}}$ is further given by $\mathbb{E}[\bar{\alpha}_{m,t} \bar{\alpha}_{n,s}^*]$, $t, s = 1, \dots, j$. From (4), we have

$$\begin{aligned} \mathbb{E}[\bar{\alpha}_{m,t} \bar{\alpha}_{n,s}^*] &= \frac{\sqrt{Q_t Q_s}}{P} \bar{\beta}_t \bar{\beta}_s \mathbb{E}[\alpha_{t,m} \alpha_{s,n}^*], \\ &\stackrel{(a)}{=} \frac{\sqrt{Q_t Q_s}}{P\tau} \bar{\beta}_t \bar{\beta}_s \delta(t-s) \delta(m-n), \end{aligned} \quad (9)$$

where (a) results from the independence of the jamming pilot sequences and the orthogonality of legitimate pilot sequences. It follows that $\Upsilon_{1:j}$ is a diagonal matrix and $[\Upsilon_{1:j}]_{\mathbf{m}, \mathbf{m}}$ is the same for any \mathbf{m} , which simplifies \mathbf{R}_y in (8) to:

$$\mathbf{R}_y = \mathbf{I}_{\tau'} \otimes \bar{\mathbf{R}}_y, \quad (10)$$

where

$$\bar{\mathbf{R}}_y = \boldsymbol{\Psi}(\boldsymbol{\theta}_{1:j}) \text{diag}\{\gamma_{1:j}\} \boldsymbol{\Psi}^H(\boldsymbol{\theta}_{1:j}) + \sigma^2 \mathbf{I}_N, \quad (11)$$

where $\boldsymbol{\gamma}_{1:j} = [\gamma_1, \dots, \gamma_j]^\top = \left[\frac{Q_1}{P} |\bar{\beta}_1|^2, \dots, \frac{Q_j}{P} |\bar{\beta}_j|^2 \right]^\top$ represents the average jamming-to-signal ratio (JSR) vector for the first j jammers to the BS antenna.

The problem in (6) is typically addressed using a GIC-based approach. Specifically, the corresponding optimization problem is formulated as [16]:

$$\mathbf{P} : \hat{J} = \arg \max_{j \in \{0, \dots, J_{\max}\}} \text{GIC}_j, \quad (12a)$$

$$\text{GIC}_j = \begin{cases} 0, & \text{if } j = 0 \\ \max_{\boldsymbol{\theta}_{1:j} \in \mathcal{G}_{1:j}} T_G(\boldsymbol{\theta}_{1:j}) - \kappa_j, & \text{if } j > 0, \end{cases} \quad (12b)$$

where the estimate \hat{J} represents the number of potential jammers, and $T_G(\boldsymbol{\theta}_{1:j}) = \max_{\boldsymbol{\gamma}_{1:j}} \ln \frac{f_j(\mathbf{y}; \boldsymbol{\theta}_{1:j}, \boldsymbol{\gamma}_{1:j})}{f_0(\mathbf{y})}$ is the generalized log-likelihood ratio (GLR), where $f_0(\mathbf{y})$ denotes the likelihood function under \mathcal{H}_0 , and κ is the penalty factor. The set $\mathcal{G}_{1:j}$ represents all possible jammer angles and is given by

$$\mathcal{G}_{1:j} = \left\{ \boldsymbol{\theta}_{1:j} = [\theta_1, \dots, \theta_j]^\top \mid \theta_p \in \mathcal{G}, \forall p = 1, \dots, j \right\}, \quad (13)$$

where \mathcal{G} is a predefined discrete grid with L equally spaced points in the interval $[-1, 1]$.

To solve problem \mathbf{P} , the typical approach is to first derive the MLE $\hat{\boldsymbol{\gamma}}_{1:j}$ of the average JSR vector. This estimate is then substituted into (13b), yielding a tractable objective function. By searching the set of candidate angles $\mathcal{G}_{1:j}$, the maximum value of the objective function GIC_j is found, which allows both the number of jammers and their corresponding angles to be determined. However, there are two major challenges. First, unlike the deterministic signal models with unknown parameters considered in [11], the stochastic signal model with unknown parameters used in (5) makes it mathematically difficult to derive the MLE of $\boldsymbol{\gamma}_{1:j}$ [17]. Second, solving the problem for each hypothesis \mathcal{H}_j requires an exhaustive search over L^j grid points, which leads to an exponential growth in computational complexity as the number of jammers increases. To address these challenges, we propose a low-complexity algorithm for joint jamming detection and angle estimation.

B. GLRT Based on Spatial Covariance Identification

Based on the likelihood function analysis of the vector \mathbf{y} in Section III-A, the composite multiple hypothesis testing problem as formulated in (6) can be equivalently transformed into a spatial covariance matrix identification problem:

$$\begin{cases} \mathcal{H}_0 : & \bar{\mathbf{R}}_y = \sigma^2 \mathbf{I}_N, \\ \mathcal{H}_1 : & \bar{\mathbf{R}}_y = \gamma_1 \boldsymbol{\Psi}(\theta_1) \boldsymbol{\Psi}^H(\theta_1) + \sigma^2 \mathbf{I}_N, \\ & \vdots \\ \mathcal{H}_{J_{\max}} : & \bar{\mathbf{R}}_y = \boldsymbol{\Psi}(\boldsymbol{\theta}_{1:J_{\max}}) \text{diag}\{\gamma_{1:J_{\max}}\} \boldsymbol{\Psi}^H(\boldsymbol{\theta}_{1:J_{\max}}) + \sigma^2 \mathbf{I}_N. \end{cases} \quad (14)$$

Using the design strategy presented in [12], we decompose the composite multiple hypothesis test in (14) into $J_{\max} - 1$ binary hypothesis tests. Specifically, the t -th (for $t = 1, \dots, J_{\max} - 1$) detection problem is formulated as follows:

$$\begin{cases} \mathcal{H}_0^{(t)} : & \bar{\mathbf{R}}_y^{(t)} = \hat{\bar{\mathbf{R}}}_y^{(t-1)} \\ \mathcal{H}_1^{(t)} : & \bar{\mathbf{R}}_y^{(t)} = \hat{\bar{\mathbf{R}}}_y^{(t-1)} + \gamma_t \boldsymbol{\Psi}(\theta_t) \boldsymbol{\Psi}^H(\theta_t), \end{cases} \quad (15)$$

where $\hat{\bar{\mathbf{R}}}_y^{(t-1)}$ is the spatial covariance matrix estimated in the $(t-1)$ -th iteration. For $t = 1$, the initial covariance matrix estimation is $\hat{\bar{\mathbf{R}}}_y^{(0)} = \sigma^2 \mathbf{I}_N$, representing a pure noise scenario.

For $t > 1$, the covariance matrix estimate $\hat{\bar{\mathbf{R}}}_y^{(t-1)}$ is updated as:

$$\hat{\bar{\mathbf{R}}}_y^{(t-1)} = \boldsymbol{\Psi}(\hat{\boldsymbol{\theta}}_{1:t-1}) \text{diag}\{\hat{\boldsymbol{\gamma}}_{1:t-1}\} \boldsymbol{\Psi}^H(\hat{\boldsymbol{\theta}}_{1:t-1}) + \sigma^2 \mathbf{I}_N, \quad (16)$$

where $\hat{\boldsymbol{\theta}}_{1:t-1}$ and $\hat{\boldsymbol{\gamma}}_{1:t-1}$ are the estimated angle vector and the corresponding JSR vector from the previous $t-1$ iterations.

The binary detections in (15) are performed sequentially. In each detection step, the system tests for the presence of a potential jammer, or equivalently, updates the spatial covariance matrix corresponding to a single jammer-BS link. The detection process continues until one of the following two conditions is met: either we conclude that $\mathcal{H}_0^{(t)}$ holds (indicating that no additional jammers are present), or we reach the maximum number of iterations, $J_{\max} - 1$. In the final round T of detection:

- If $\mathcal{H}_0^{(T)}$ is declared, then $T-1$ jammers have been detected.
- If $\mathcal{H}_1^{(T)}$ is declared, then T jammers are present.

It can be observed that the covariance matrix estimation $\hat{\mathbf{R}}_{\mathbf{y}}^{(t-1)}$ is a deterministic matrix in the t -th binary detection, which is determined by the estimated angles and JSRs of the first $t-1$ jammers. With the given matrix $\hat{\mathbf{R}}_{\mathbf{y}}^{(t-1)}$, the detection problem in (15) reduces to a test of two scalar parameters: the average JSR γ_t and the spatial angle θ_t . To implement the GLRT, we first represent the log-likelihood function of the vector \mathbf{y} under $\mathcal{H}_1^{(t)}$ as

$$\begin{aligned} & \ln f_1^{(t)}(\mathbf{y}; \hat{\boldsymbol{\theta}}_{1:t-1}, \hat{\boldsymbol{\gamma}}_{1:t-1}, \theta_t, \gamma_t) \\ &= -\tau' N \ln \pi - \tau' \ln \left| \bar{\mathbf{R}}_{\mathbf{y}}^{(t)} \right| - \mathbf{y}^H \left(\mathbf{I}_{\tau'} \otimes \left(\bar{\mathbf{R}}_{\mathbf{y}}^{(t)} \right)^{-1} \right) \mathbf{y}. \end{aligned} \quad (17)$$

Based on (15), and by applying Woodbury's matrix identity and the matrix determinant lemma [18], we derive the closed-form expressions for the inverse and determinant of $\bar{\mathbf{R}}_{\mathbf{y}}^{(t)}$ under $\mathcal{H}_1^{(t)}$ as follows:

$$\begin{aligned} \left(\bar{\mathbf{R}}_{\mathbf{y}}^{(t)} \right)^{-1} &= \left(\hat{\mathbf{R}}_{\mathbf{y}}^{(t-1)} \right)^{-1} \\ &- \frac{\gamma_t}{1 + \gamma_t R(\theta_t)} \left(\hat{\mathbf{R}}_{\mathbf{y}}^{(t-1)} \right)^{-1} \boldsymbol{\Psi}(\theta_t) \boldsymbol{\Psi}^H(\theta_t) \left(\hat{\mathbf{R}}_{\mathbf{y}}^{(t-1)} \right)^{-1}, \end{aligned} \quad (18)$$

and

$$\left| \bar{\mathbf{R}}_{\mathbf{y}}^{(t)} \right| = (1 + \gamma_t R(\theta_t)) \left| \hat{\mathbf{R}}_{\mathbf{y}}^{(t-1)} \right|, \quad (19)$$

where

$$R(\theta_t) = \boldsymbol{\Psi}^H(\theta_t) \left(\hat{\mathbf{R}}_{\mathbf{y}}^{(t-1)} \right)^{-1} \boldsymbol{\Psi}(\theta_t). \quad (20)$$

By utilizing (18) and (19) in (17), the log-likelihood function in (17) can be further expressed as

$$\begin{aligned} \ln f_1^{(t)}(\mathbf{y}; \hat{\boldsymbol{\theta}}_{1:t-1}, \hat{\boldsymbol{\gamma}}_{1:t-1}, \theta_t, \gamma_t) &= \ln f_0^{(t)}(\mathbf{y}; \hat{\boldsymbol{\theta}}_{1:t-1}, \hat{\boldsymbol{\gamma}}_{1:t-1}) \\ &- \tau' \ln(1 + \gamma_t R(\theta_t)) + \frac{\gamma_t}{1 + \gamma_t R(\theta_t)} Q(\theta_t), \end{aligned} \quad (21)$$

where $\ln f_0^{(t)}(\mathbf{y}; \hat{\boldsymbol{\theta}}_{1:t-1}, \hat{\boldsymbol{\gamma}}_{1:t-1})$ is the log-likelihood function of the vector \mathbf{y} under $\mathcal{H}_0^{(t)}$, and

$$Q(\theta_t) = \mathbf{y}^H \left(\mathbf{I}_{\tau'} \otimes \left(\left(\hat{\mathbf{R}}_{\mathbf{y}}^{(t-1)} \right)^{-1} \boldsymbol{\Psi}(\theta_t) \boldsymbol{\Psi}^H(\theta_t) \left(\hat{\mathbf{R}}_{\mathbf{y}}^{(t-1)} \right)^{-1} \right) \right) \mathbf{y}. \quad (22)$$

Algorithm 1 Implementation of the GLRT-SCI Scheme

- 1: **Input:** \mathcal{G} , $\kappa_G \geq 0$, J_{\max} , $\hat{J} = 0$, $\hat{\boldsymbol{\theta}} = []$
 - 2: **Output:** \hat{J} and $\hat{\boldsymbol{\theta}}$
 - 3: Generate $\boldsymbol{\Psi}(\theta_p)$'s for all $\theta_p \in \mathcal{G}$
 - 4: **for** $t = 1, \dots, J_{\max} - 1$ **do**
 - 5: Compute $\hat{\mathbf{R}}_{\mathbf{y}}^{(t-1)}$ from (16)
 - 6: Calculate $R(\theta_t)$ and $Q(\theta_t)$ from (20) and (22)
 - 7: Determine $T_G^{(t)}(\theta_t)$ from (25)
 - 8: **if** $\max_{\theta_t \in \mathcal{G}} T_G^{(t)} \geq \kappa_G$ **then**
 - 9: $\hat{\theta}_t = \arg \max_{\theta_t \in \mathcal{G}} T_G^{(t)}$; $\hat{\boldsymbol{\theta}} = [\hat{\boldsymbol{\theta}}; \hat{\theta}_t]$; $\hat{J} = \hat{J} + 1$
 - 10: **else**
 - 11: **break**
 - 12: **end if**
 - 13: **end for**
-

According to (21), we have

$$\begin{aligned} & \frac{\partial \ln f_1^{(t)}(\mathbf{y}; \hat{\boldsymbol{\theta}}_{1:t-1}, \hat{\boldsymbol{\gamma}}_{1:t-1}, \theta_t, \gamma_t)}{\partial \gamma_t} \\ &= -\frac{\tau' R(\theta_t)}{1 + \gamma_t R(\theta_t)} + \frac{Q(\theta_t)}{(1 + \gamma_t R(\theta_t))^2}. \end{aligned} \quad (23)$$

Differentiating (23) with respect to γ_t and setting to 0 gives the MLE as

$$\hat{\gamma}_t = \frac{Q(\theta_t) - \tau' R(\theta_t)}{\tau' R^2(\theta_t)}. \quad (24)$$

After plugging (24) into the log-likelihood ratio, the detection metric at the t -th iteration is given by

$$\begin{aligned} T_G^{(t)}(\theta_t) &= \ln \frac{f_1^{(t)}(\mathbf{y}; \hat{\boldsymbol{\theta}}_{1:t-1}, \hat{\boldsymbol{\gamma}}_{1:t-1}, \theta_t, \hat{\gamma}_t)}{f_0^{(t)}(\mathbf{y}; \hat{\boldsymbol{\theta}}_{1:t-1}, \hat{\boldsymbol{\gamma}}_{1:t-1})}, \\ &= -\tau' \ln(1 + \hat{\gamma}_t R(\theta_t)) + \frac{\hat{\gamma}_t Q(\theta_t)}{1 + \hat{\gamma}_t R(\theta_t)}, \\ &= -\tau' \ln \left(\frac{Q(\theta_t)}{\tau' R(\theta_t)} \right) + \frac{Q(\theta_t)}{R(\theta_t)} - \tau'. \end{aligned} \quad (25)$$

The detection rule for the t -th iteration is as follows

$$\max_{\theta_t \in \mathcal{G}} T_G^{(t)}(\theta_t) \underset{\mathcal{H}_0^{(t)}}{\overset{\mathcal{H}_1^{(t)}}{\geq}} \kappa_G, \quad (26)$$

where $\kappa_G \geq 0$ is the detection threshold, which can be set numerically given a constant false-alarm probability $P_F = \Pr \left(\max_{\theta_t \in \mathcal{G}} T_G^{(t)}(\theta_t) > \kappa_G | \mathcal{H}_0 \right)$ [11]. The procedure is referred to as the GLRT-SCI and is summarized in Algorithm 1.

C. Benchmarks and Complexity Analysis

Two benchmarks are considered for comparison. The first one is the matched subspace detector (MSD) with iterative estimation of the interference subspace (MSD-IS) [12], and the second one is the MSD with iterative estimation of the interference covariance matrix (MSD-ICM) [11]. To solve our problem, these detectors require appropriate modifications.

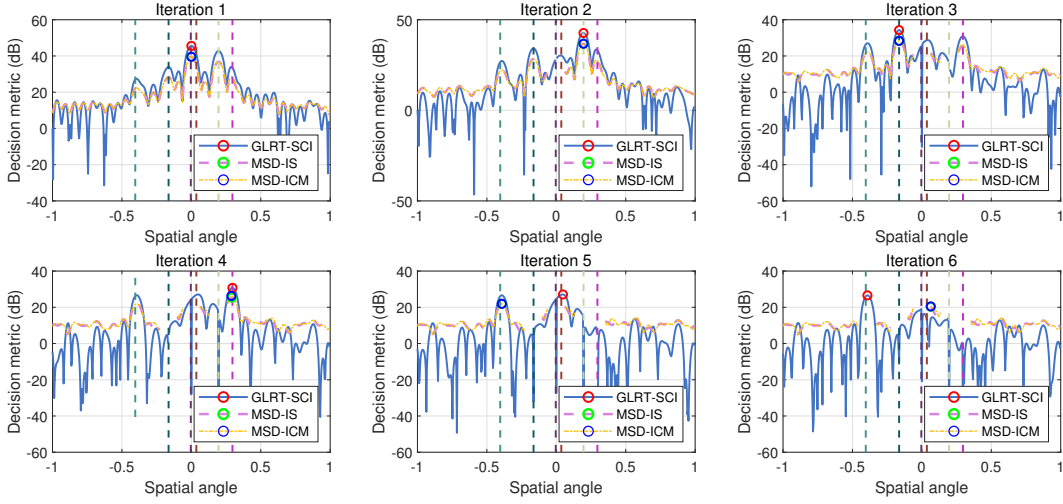


Fig. 1: The log-scale decision metrics in (25) and (27) under 6 iterations, where the JNR = 20 dB, the grid size $L = 500$, the false-alarm probability $P_F = 10^{-3}$, and the number of unused pilots $\tau' = 9$. The vertical dashed lines indicate the true spatial angles of the jammers, and the red, green, and blue circles mark the estimated angles at each iteration under the three detection schemes.

Specifically, the modified detector at iteration t can be expressed as

$$\max_{\theta_t \in \mathcal{G}} T_{\text{MSD}}^{(t)}(\theta_t) = \max_{\theta_t \in \mathcal{G}} \frac{\mathbf{y}^H \left(\mathbf{I}_{\tau'} \otimes \left(\mathbf{\Pi}^{(t)}(\theta_t) \left(\mathbf{\Pi}^{(t)}(\theta_t) \right)^H \right) \right) \mathbf{y}}{\left\| \mathbf{\Pi}^{(t)}(\theta_t) \right\|^2} \underset{\mathcal{H}_0^{(t)}}{\overset{\mathcal{H}_1^{(t)}}{\gtrless}} \kappa_{\text{SD}}, \quad (27)$$

where $\kappa_{\text{SD}} \geq 0$ is the threshold, and $\mathbf{\Pi}^{(t)}(\theta_t) = \mathbf{\Xi}^{(t)} \mathbf{\Psi}(\theta_t)$, where $\mathbf{\Xi}^{(t)}$ is a projection matrix that distinguishes between the MSD-IS and MSD-ICM approaches, defined as:

$$\mathbf{\Xi}^{(t)} = \begin{cases} \mathbf{I}_N - \mathbf{\Psi}(\hat{\theta}_{1:t-1}) \mathbf{\Psi}^\dagger(\hat{\theta}_{1:t-1}), & \text{MSD-IS} \\ \left(\mathbf{\Psi}(\hat{\theta}_{1:t-1}) \hat{\mathbf{\Gamma}}_{1:t-1} \mathbf{\Psi}^H(\hat{\theta}_{1:t-1}) + \sigma^2 \mathbf{I}_N \right)^{-1/2}, & \text{MSD-ICM} \end{cases} \quad (28)$$

where $\hat{\mathbf{\Gamma}}_{1:t-1}$ is a diagonal matrix representing the intensity of the jamming, which must be re-estimated at each iteration.

Next, we analyze the computational complexity of the GLRT-SCI scheme compared to the benchmarks. The pre-generation of $\mathbf{\Psi}(\theta_p)$'s requires $\mathcal{O}(NMP)$ floating-point operations (flops), which is a common cost for all algorithms. For the proposed scheme, each iteration involves $\mathcal{O}(N^2)$ flops to compute $\hat{\mathbf{R}}_{\mathbf{y}}^{(t-1)}$ and its inverse as described in (18), and $\mathcal{O}(N^2P)$ flops to compute $R(\theta_t)$ and $Q(\theta_t)$. As a result, the total computational cost for evaluating (26) is $\mathcal{O}(NMP + N^2P)$. For the MSD-type algorithms, the main computational differences arise from the calculation of the projection matrix in (28). Specifically, the MSD-IS requires pseudo-inversion and matrix multiplication, with a complexity of $\mathcal{O}(t^3 + Nt^2 + N^2t)$, while the MSD-ICM involves the estimation of $\hat{\mathbf{\Gamma}}_{1:t}$ and matrix inversion, resulting in a higher complexity of $\mathcal{O}(t^3 + Nt^2 + N^2t + N^3)$. Including the computations in (27), the total costs of the two MSD-type algorithms are $\mathcal{O}(NMP + N^2(P + t) + Nt^2 + t^3)$ and $\mathcal{O}(NMP + N^3 + N^2(P + t) + Nt^2 + t^3)$, respectively. As the number of iterations and RF chains increases, the proposed

scheme achieves JDAE with a slightly lower computational complexity compared to these MSD-based approaches.

IV. SIMULATIONS AND DISCUSSIONS

In this section, we provide simulation results to evaluate the performance of our proposed scheme and benchmarks. We consider a simulation scenario where the BS is positioned at the origin of the coordinate system $(0, 0)$. A user and $J = 6$ jammers are located at distances between 1 km and 1.5 km from the BS. Their physical angles relative to the BS are uniformly distributed within the range $[-\frac{\pi}{2}, \frac{\pi}{2}]$. The BS is equipped with $M = 128$ antennas and $N = 32$ RF chains. Each jammer is equipped with $M' = 4$ antennas with its analog beam perfectly aligned with the BS. At the BS, we employ the discrete Fourier transform (DFT) beamspace framework, i.e., $\mathbf{W} = [\mathbf{a}(\hat{\theta}_1), \dots, \mathbf{a}(\hat{\theta}_N)]^H$, where $\hat{\theta}_n = -1 + (n-1) \frac{2}{N}$ for $n = 1, \dots, N$. A carrier frequency $f_c = 28$ GHz is considered. The fading coefficient of the BS-jammer link is modeled as $\beta_j [\text{dB}] = -20 \lg \left(\frac{4\pi f_c}{c} \right) - 10\theta \lg(d_j) - A_\zeta$, where d_j is the distance from jammer j to the BS, and c is the speed of light. We consider a path loss exponent θ of 2 and a deviation ζ of the shadow fading factor A_ζ of 4 dB [19]. The JNR is defined as $\text{JNR} = Q_o \beta_o$, where $o = \arg \min_j \beta_j$ denotes the index of the jammer with the smallest fading coefficient to the BS. Also, the JSR is set to 0 dB, i.e., $P = Q_o$.

The probability of detection P_D and the average root mean square error (RMSE) are used as performance metrics for detection and angle estimation. The detection probability is defined as: $P_D = \mathbb{E}_j [\Pr \{E_j | \tilde{\mathcal{H}}_0\}]$, where E_j denotes the event that the j -th jammer is detected, and is defined as $E_j = \{|\hat{\theta}_j - \theta_j| \leq 2/N\}$, where $\hat{\theta}_j = \arg \min_{\hat{\theta}_p \in \{\hat{\theta}_1, \dots, \hat{\theta}_j\}} |\hat{\theta}_p - \theta_j|$ represents the estimated angle for the j -th jammer. $\tilde{\mathcal{H}}_0$ is the alternative hypothesis to \mathcal{H}_0 . Then, the average RMSE of the angle estimates is denoted as $\text{RMSE} = \sqrt{\mathbb{E}_j [|\hat{\theta}_j - \theta_j|^2 | E_j, \tilde{\mathcal{H}}_0]}$. The Monte-Carlo trials are performed to obtain the thresholds κ_G and κ_{SD} with a given false-alarm probability P_F .

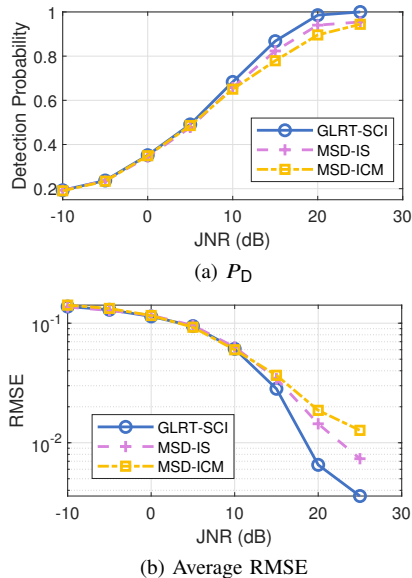


Fig. 2: The P_D and the average RMSE of the GLRT-SCI scheme, the MSD-IS scheme, and the MSD-ICM scheme versus JNR.

Fig. 1 illustrates the logarithmic-scale decision metrics of three detection schemes, with parameters set as $JNR = 20$ dB, $L = 500$, $P_F = 10^{-3}$, and $\tau' = 9$. The results demonstrate that all three algorithms can effectively detect jammers and estimate their corresponding spatial angles, even if the estimation order is different. From the observed nulls corresponding to the true angles, it is clear that the GLRT-SCI scheme effectively mitigates the mainlobe effect caused by previously detected jammers. An interesting observation is that the MSD-type methods show smaller fluctuations in the decision metrics over all angles compared to the GLRT-SCI scheme. This is because the decision metric of the GLRT-SCI, as shown in (25), includes a logarithmic term that converges the decision values to zero at angles where $\frac{Q(\theta_i)}{R(\theta_i)}$ approaches τ' , significantly increasing the disparity between true and irrelevant angles. This feature allows the GLRT-SCI to better suppress sidelobes from previously detected jammers and interference from irrelevant angles.

Fig. 2 shows the P_D and the RMSE for three schemes, where $L = 500$, $P_F = 10^{-3}$ and $\tau' = 9$. As the JNR increases, the proposed scheme shows a performance advantage over the other detectors. Specifically, at $JNR = 15$ dB, the detection probability of the proposed scheme is improved by 5.47%, and the average RMSE of the estimated angles is degraded by 23.16% compared to the MSD-IS scheme. It is noted that the MSD-IS outperforms the MSD-ICM, which is inconsistent with the phenomenon observed in [11]. This inconsistency may be due to the fact that the matrix $\hat{\mathbf{F}}_{1:\tau-1}$ in (28) is not an MLE, which makes the projection matrix suboptimal. In addition, the average RMSE in Fig. 2 and the results of 5-6 iterations in Fig. 1 consistently show that the proposed method is more accurate in estimating closely spaced jammers under medium-to-high JNRs compared to other methods.

V. CONCLUSIONS

This paper studied the JDAE problem of multiple random jammers in beamspace MIMO communication systems. By

analyzing the likelihood function of the projected vector, the original problem was transformed into multiple binary spatial covariance identification problems. An iterative low-complexity GLRT scheme was proposed, and closed-form expressions for the MLE of the average JSR and the logarithmic GLR were derived. In each iteration, the detector searches for angles to extract a single target while suppressing the mainlobe effects from previously detected jammers. Simulations showed that the proposed method outperforms benchmarks in terms of detection probability and average RMSE under medium-to-high JNRs.

REFERENCES

- [1] Z. Wang, C. Zhang, C. Zhang, and Y. Huang, "Anti-jamming transmission of downlink cell free millimeter-wave MIMO system," *arXiv preprint arXiv:2409.13261*, 2024.
- [2] X. Qi, M. Peng, H. Zhang, and X. Kong, "Anti-jamming hybrid beamforming design for millimeter-wave massive MIMO systems," *IEEE Trans. Wirel. Commun.*, vol. 23, no. 8, pp. 9160–9172, Aug. 2024.
- [3] H. Pirayesh and H. Zeng, "Jamming attacks and anti-jamming strategies in wireless networks: A comprehensive survey," *IEEE Commun. Surv. Tutor.*, vol. 24, no. 2, pp. 767–809, Mar. 2022.
- [4] J. Vinogradova, E. Björnson, and E. G. Larsson, "Detection and mitigation of jamming attacks in massive MIMO systems using random matrix theory," in *Proc. IEEE Workshop Signal Process. Adv. Wirel. Commun. (SPAWC)*, Edinburgh, United Kingdom, Jul. 2016, pp. 1–5.
- [5] H. Akhlaghpasand, S. M. Razavizadeh, E. Björnson, and T. T. Do, "Jamming detection in massive MIMO systems," *IEEE Wirel. Commun. Lett.*, vol. 7, no. 2, pp. 242–245, Apr. 2017.
- [6] D. Kapetanović, G. Zheng, K.-K. Wong, and B. Ottersten, "Detection of pilot contamination attack using random training and massive MIMO," in *Proc. IEEE Int. Symp. Person Indoor Mobile Radio Commun. (PIMRC)*, London, United Kingdom, Sep. 2013, pp. 13–18.
- [7] P. Du, C. Zhang, Y. Jing, C. Fang, Z. Zhang, and Y. Huang, "Jamming detection and channel estimation for spatially correlated beamspace massive MIMO," *arXiv preprint arXiv:2410.14215*, 2024.
- [8] H. Akhlaghpasand, E. Björnson, and S. M. Razavizadeh, "Jamming suppression in massive MIMO systems," *IEEE Trans. Circuits Syst. II-Express Briefs*, vol. 67, no. 1, pp. 182–186, Jan. 2020.
- [9] T. T. Do, E. Björnson, E. G. Larsson, and S. M. Razavizadeh, "Jamming-resistant receivers for the massive MIMO uplink," *IEEE Trans. Inf. Forensic Secur.*, vol. 13, no. 1, pp. 210–223, Jan. 2018.
- [10] S. Bagherinejad and S. M. Razavizadeh, "Direction-based jamming detection and suppression in mmWave massive MIMO networks," *IET Commun.*, vol. 15, no. 14, pp. 1780–1790, Apr. 2021.
- [11] Y. Lai, L. Venturino, E. Grossi, and W. Yi, "Joint detection and localization in distributed MIMO radars employing waveforms with imperfect auto- and cross-correlation," *IEEE Trans. Veh. Technol.*, 2023.
- [12] Y. Lai, L. Venturino, E. Grossi, and W. Yi, "Subspace-based detection and localization in distributed MIMO radars," in *Proc. IEEE Sens. Array Multichannel Signal Process. Workshop (SAM)*, Trondheim, Norway, June 2022, pp. 365–369.
- [13] Y. Cai, C. Zhao, Q. Shi, G. Y. Li, and B. Champagne, "Joint beamforming and jamming design for mmWave information surveillance systems," *IEEE J. Sel. Areas Commun.*, vol. 36, no. 7, pp. 1410–1425, 2018.
- [14] Z. Xiao, H. Dong, L. Bai, D. O. Wu, and X.-G. Xia, "Unmanned aerial vehicle base station (UAV-BS) deployment with millimeter-wave beamforming," *IEEE Internet Things J.*, vol. 7, no. 2, pp. 1336–1349, 2019.
- [15] J. Tan, T. H. Luan, W. Guan, Y. Wang, H. Peng, Y. Zhang, D. Zhao, and N. Lu, "Beam alignment in mmwave V2X communications: A survey," *IEEE Commun. Surv. Tutor.*, 2024.
- [16] E. Grossi, M. Lops, A. M. Tulino, and L. Venturino, "Opportunistic sensing using mmWave communication signals: A subspace approach," *IEEE Trans. on Wirel. Commun.*, vol. 20, no. 7, pp. 4420–4434, 2021.
- [17] S. M. Kay, "Fundamentals of statistical signal processing," 1993.
- [18] D. A. Harville, "Matrix algebra from a statistician's perspective," 1998.
- [19] P. Xin, Y. Cao, Y. Wu, D. Wang, X. You, and J. Wang, "Hybrid precoding with per-beam timing advance for asynchronous cell-free mmWave massive MIMO-OFDM systems," *arXiv preprint arXiv:2411.05305*, 2024.